Supporting Information

Light- and Radical-Induced Modification of Magnetic and Magnetocaloric Effects in Viologen-Based Lanthanide Materials

Hao Wang,[a] Tian-Tian Wang,[a] Zhao-Bo Hu,[b] Sui-Jun Liu*[b] and Wen-Bin Sun*[a]

[a] Key Laboratory of Functional Inorganic Material Chemistry Ministry of Education, School of Chemistry and Material Science Heilongjiang University, 74 Xuefu Road, Harbin 150080, P. R. China.

[b] School of Chemistry and Chemical Engineering, Jiangxi Provincial Key Laboratory of Functional Crystalline Materials Chemistry, Jiangxi University of Science and Technology, Ganzhou 341000, Jiangxi, P. R. China.

[a]*E-mail: wenbinsun@126.com

[b]*E-mail: sjliu@jxust.edu.cn

Experimental Section

Materials and Reagents

All reagents and solvents were purchased commercially and used without further purification.

Synthesis of *N, N′*-4, 4′-Bipyridinio-dipropionate ($H_2BpydpCl_2$)

The *N, N*'-4, 4'-Bipyridinio-dipropionate ligand was synthesized according to previously reported methods.[1]

Synthesis of [(Bpydp)Dy(H_2O)(PTA)]·NO_3·2H_2O (1-Dy)

The synthesis method follows our previous work, with only the rare-earth salt being modified.[2] A mixture of 0.1 mmol (37.2 mg) of $H_2BpydpCl_2$, 0.1 mmol (16.6 mg) of *p*-Phthalic acid (H_2PTA), 0.1 mmol (44.6 mg) of $Dy(NO_3)_3·6H_2O$, 4 mL ethanol, 2 mL *N, N* -dimethylformamide, and 2 mL H_2O was placed in a closed 25 mL Teflon-lined autoclave. The mixture was heated at 80 °C for 72 h and then cooled to room temperature naturally. Faint yellow rod-shaped crystals were collected by filtration, yielding 48% (based on Dy^{III}). Selected IR data (KBr, cm^{-1}): 3414 (w), 3126 (w), 2438 (w), 1594 (s), 1502 (m), 1448 (s), 1373 (m), 1150 (w), 950 (w), 884 (m), 830 (m), 752 (m), 673 (w), 572 (w). Elemental analysis (wt %): calculated for $C_{24}H_{26}DyN_3O_{14}$: C, 38.80; H, 3.53; N, 5.66. Found: C, 38.72; H, 3.61; N, 5.71.

Synthesis of [(Bpydp)Gd(H_2O)(PTA)]·NO_3·2H_2O (1-Gd)

The synthesis method is identical to 1-Dy, with the only modification being substituting the rare-earth nitrate salt with 0.1 mmol (45.1 mg) of $Gd(NO_3)_3·6H_2O$. Faint yellow rod-shaped crystals were collected by filtration, with a yield of 62%. Selected IR data

(KBr, cm^{-1}): 3413 (w), 3125 (w), 2438 (w), 1592 (s), 1503 (m), 1447 (s), 1373 (m), 1150 (w), 951 (w), 884 (m), 829 (m), 753 (m), 674 (w), 574 (w). Elemental analysis (wt %): calculated for $C_{24}H_{26}GdN_3O_{14}$: C, 39.07; H, 3.55; N, 5.70. Found: C, 38.99; H, 3.62; N, 5.75.

Synthesis of $[(Bpydp)_{0.5}Dy_2(IPA)_3]_n$ (2-Dy)

The synthesis method follows that of Zheng et al., with the only modification being substituting the rare-earth salt.[3] A mixture of 0.05 mmol (18.6 mg) of $H_2BpydpCl_2$, 0.15 mmol (24.9 mg) of Isophthalic acid (H_2IPA), 0.15 mmol (66.9 mg) of $Dy(NO_3)_3 \cdot 6H_2O$, 2 mL ethanol, 2 mL *N, N* -dimethylformamide, and 4 mL of NaOH (0.05 mol/L) was placed in a closed 25 mL Teflon-lined autoclave. The mixture was heated at 100 °C for 48 h and then cooled to room temperature naturally. Colorless rod-shaped crystals were collected by filtration, yielding 72% (based on Dy^{III}). Selected IR data (KBr, cm^{-1}): 3657 (w), 3083 (w), 3056 (w), 1618 (s), 1574 (m), 1547 (s), 1483 (w), 1452 (s), 1393 (s), 1156 (w), 1071 (w), 834 (w), 752 (m), 713 (m), 649 (w), 582 (w), 543 (w). Elemental analysis (wt %): calculated for $C_{32}H_{20}Dy_2NO_{14}$: C, 39.73; H, 2.08; N, 1.45. Found: C, 39.82; H, 2.03; N, 1.52.

Characterization

Powder X-ray diffraction (PXRD) patterns were recorded on a Bruker-D8 diffractometer with Cu-Kα radiation. Fourier transform infrared (FTIR) spectra were obtained using a Perkin-Elmer Spectrum One spectrometer with KBr pellets. Electron paramagnetic resonance (EPR) measurements were performed on a Bruker EMXplus spectrometer. UV-vis diffuse reflectance spectra were measured using a Lambda 900

instrument, with $BaSO_4$ serving as the reference material. A PLS-SXE300D 300 W Xenon lamp system equipped with a PLS-BP20365 (365 nm filter) was used for photochromic studies. The sample was placed 10 cm from the xenon lamp during irradiation. After irradiation, the solid-state UV-vis diffuse reflectance of the irradiated sample was subsequently measured.

Computational Details

The spin population analysis in this study was performed using a combination of Gaussian 16, ORCA 6.0.0, and Multiwfn 3.8 (dev). [4-8] The structures of **1-Dy** and **2-Dy** were directly obtained from experimental measurements, while the structure of **1-Gd** was generated by replacing the Dy atom with Gd, followed by structural optimization.

Single-Radical system: To consider the possible location of a single radical in the system, a 4f fully occupied, nonmagnetic Lu atom was used instead of Dy, and a large-core pseudopotential was employed to shield all 4f electrons, thus ensuring that only one spin electron remains in the system. For complex **1**, the asymmetric unit was used as the initial structure; for complex **2**, the asymmetric unit was completed by reconstructing the bipyridine moiety. Single-point energy evaluations were conducted at the PBE0/6-31G* level for C, H, O, and N atoms and at the PBE0/MWB60 level for the Lu atom. Dispersion corrections were applied using BJ damping. The isosurface maps of spin density distribution were exported using the VESTA software.[9]

Ln-Radical system: For complexes **1-Dy** and **1-Gd** in the Ln–Radical system, single-point energy calculations were performed using the asymmetric unit as the initial structure. The O3LYP/def2-TZVP level of theory was applied to all atoms, with ZORA

relativistic corrections considered for heavy atoms (Dy, Gd). The SARC/J auxiliary Coulomb fitting basis set was employed to enhance computational efficiency. TightSCF convergence criteria and the DEFGRID3 integration grid were utilized to ensure robust convergence and reliable results. Spin-density isosurface maps were visualized using VMD 1.9.4.[10]

Table S1 Crystallographic data and structural refinements parameters for **1-Dy**, **2-Dy**.

Complex	**1-Dy**	**2-Dy**
Formula	$C_{24}H_{26}DyN_3O_{14}$	$C_{32}H_{20}Dy_2NO_{14}$
*M*r (g·mol^{-1})	742.98	967.49
Temperature/*K*	293	293
Space group	*Pbca*	$P2_1/c$
Crystal system	orthorhombic	monoclinic
a (Å)	14.666(2)	10.7786(6)
b (Å)	18.530(3)	13.8101(7)
c (Å)	19.784(3)	22.0003(9)
α (°)	90	90
β (°)	90	102.801(5)
γ (°)	90	90
V (Å^3)	5376.4(15)	3193.4(3)
Z	8	4
F (000)	2952.0	1852.0
D_c (g·cm^{-3})	1.836	2.012
μ (mm^{-1})	2.858	4.717
R_{int}	0.0338	0.1091
limiting indice	$-15 \le h \le 17$	$-13 \le h \le 13$
Collected reflections	32555	22059
Unique reflections	5068	7481
GOF on F^2	1.069	1.049
R_1, wR_2 [I>2σ(I)]	0.0294 0.0655	0.0904 0.1748
R_1, wR_2 [all data]	0.0429 0.0706	0.1398 0.1981

$^aR_1 = \Sigma||F_0| - |F_c||/\Sigma|F_o|$. $^bwR_2 = \Sigma[w(F_0^2 - F_c^2)^2]/\Sigma[w(F_0^2)^2]^{1/2}$.

Table S2 Calculation results for **1-Dy** and **2-Dy** using SHAPE 2.1 software.

1-Dy(Dy1)	Structure	2-Dy(Dy1)	Structure	2-Dy(Dy2)	Structure
OP-8	30.521	**OP-8**	30.100	**HP-7**	32.345
HPY-8	21.726	**HPY-8**	21.589	**HPY-7**	21.142
HBPY-8	14.332	**HBPY-8**	12.579	**PBPY-7**	6.596
CU-8	11.642	**CU-8**	11.033	**COC-7**	1.948
SAPR-8	2.896	**SAPR-8**	6.385	**CTPR-7**	1.826
TDD-8	2.257	**TDD-8**	4.160	**JPBPY-7**	9.387
JGBF-8	11.918	**JGBF-8**	10.219	**JETPY-7**	18.389
JETBPY-8	26.603	**JETBPY-8**	20.435		
JBTPR-8	2.923	**JBTPR-8**	3.242		
BTPR-8	2.476	**BTPR-8**	3.219		
JSD-8	3.373	**JSD-8**	4.674		
TT-8	12.409	**TT-8**	11.581		
ETBPY-8	22.550	**ETBPY-8**	17.982		

Table S3 The shortest donor-acceptor distances in **1-Dy**.

Complex	Donor	Acceptor	d(D···A)/Å
1-Dy	O1	N1	3.375
1-Dy	O3	N2	3.095
1-Dy	O6	N2	3.324

Table S4 Bond Lengths for **1-Dy**.

Atom	Atom	Length/Å
Dy1	O1	2.272(3)
Dy1	O2[2]	2.338(3)
Dy1	O3[3]	2.464(3)
Dy1	O4[3]	2.385(3)
Dy1	O5	2.245(3)
Dy1	O7[1]	2.481(3)
Dy1	O8[1]	2.420(3)
Dy1	O9	2.376(3)

[1]1-X,-1/2+Y,1/2-Z; [2]1-X,1-Y,1-Z; [3]+X,3/2-Y,-1/2+Z

Table S5 Bond Angles for **1-Dy**.

Atom	Atom	Atom	Angle/°	Atom	Atom	Atom	Angle/°
O8[1]	Dy1	O7	53.42(9)	O2[3]	Dy1	O4[2]	151.37(11)
O8[1]	Dy1	O3	128.41(10)	O2[3]	Dy1	O9	75.74(12)
O5	Dy1	O7	81.70(11)	O3[2]	Dy1	O7[1]	123.00(9)
O5	Dy1	O8	134.88(10)	O4[2]	Dy1	O7[1]	76.34(10)
O5	Dy1	O1	148.55(11)	O4[2]	Dy1	O8[1]	80.10(11)
O5	Dy1	O2	85.14(10)	O4[2]	Dy1	O3[2]	53.98(10)
O5	Dy1	O3	77.29(10)	O9	Dy1	O7[1]	147.70(11)
O5	Dy1	O4	95.09(11)	O9	Dy1	O8[1]	133.27(11)
O5	Dy1	O9	81.77(13)	O9	Dy1	O3[2]	79.66(11)
O1	Dy1	O7	129.21(10)	O9	Dy1	O4[2]	132.72(11)
O1	Dy1	O8	76.53(10)	O1	Dy1	O9	73.27(12)
O1	Dy1	O2	106.34(11)	O2[3]	Dy1	O7[1]	75.37(11)
O1	Dy1	O3	79.62(10)	O2[3]	Dy1	O8[1]	79.64(11)
O1	Dy1	O4	88.27(11)	O2[3]	Dy1	O3[2]	151.52(11)

Table S6 Magnetic relaxation energy barriers derived from Orbach process (eq. 3) fitting under zero field and 1500 Oe dc-field.

Complex	U_{eff}/k_B	τ_0(s)	R^2
1-Dy (0 Oe)	57.98	1.016×10^{-6}	0.999
1-Dy-a (0 Oe)	75.46	1.269×10^{-7}	0.970
1-Dy (1500 Oe)	54.26	8.655×10^{-7}	0.994
1-Dy-a (1500 Oe)	60.76	3.662×10^{-7}	0.995

Table S7 Magnetic relaxation energy barriers derived from Orbach process, Raman process and QTM (eqs. 3-5) fitting under zero field.

Complex(0 Oe)	U_{eff}/k_B	τ_0(s)	R^2
1-Dy (Raman+Orbach+QTM)	68.93	7.98×10^{-7}	1.000
1-Dy-a (Raman+Orbach+QTM)	84.02	9.14×10^{-8}	0.999
1-Dy-a (Raman+Orbach)	84.20	7.05×10^{-8}	0.998

Table S8 Magnetic relaxation energy barriers derived from Orbach process and Raman process (eqs. 3-4) fitting under 1500 Oe dc-field.

Complex(1500 Oe)	U_{eff}/k_B	τ_0(s)	R^2
1-Dy (Raman+Orbach)	64.42	4.31×10^{-7}	1.000
1-Dy-a (Raman+Orbach)	70.33	1.55×10^{-7}	1.000

Table S9 The exchange coupling constants *J* of **1-Dy** and **1-Gd** obtained from theoretical calculations.

Complex	Spin-projection(cm^{-1})	Non-Spin projection(cm^{-1})
1-Dy	24.75	20.87
1-Gd	-5.23	-4.60

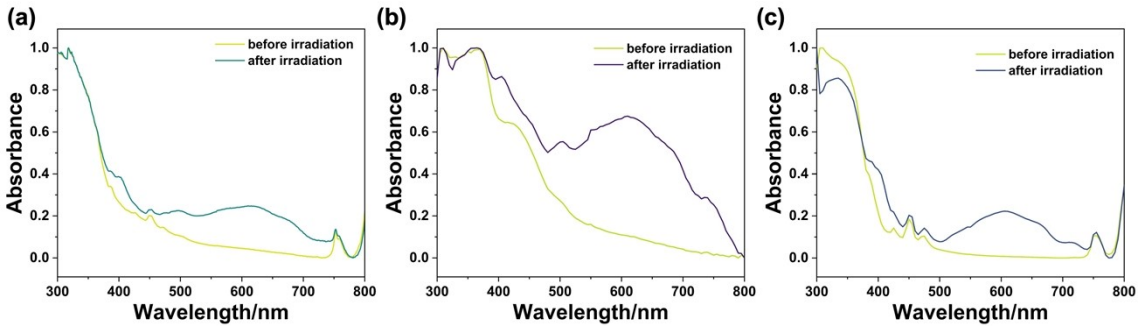

Fig. S1 UV-vis spectra of **1-Dy** (a), **1-Gd** (b) and **2-Dy** (c) before and after irradiation.

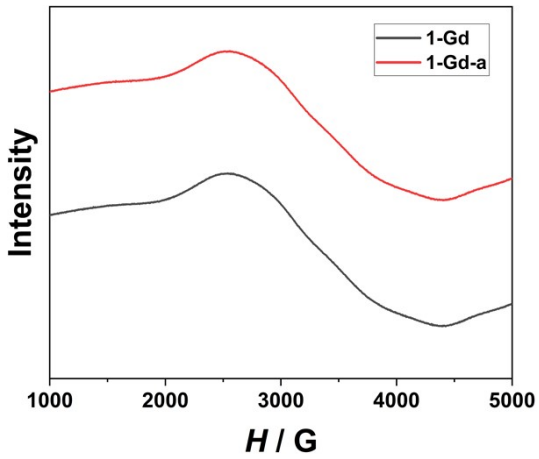

Fig. S2 EPR spectra of **1-Gd** and **1-Gd-a**.

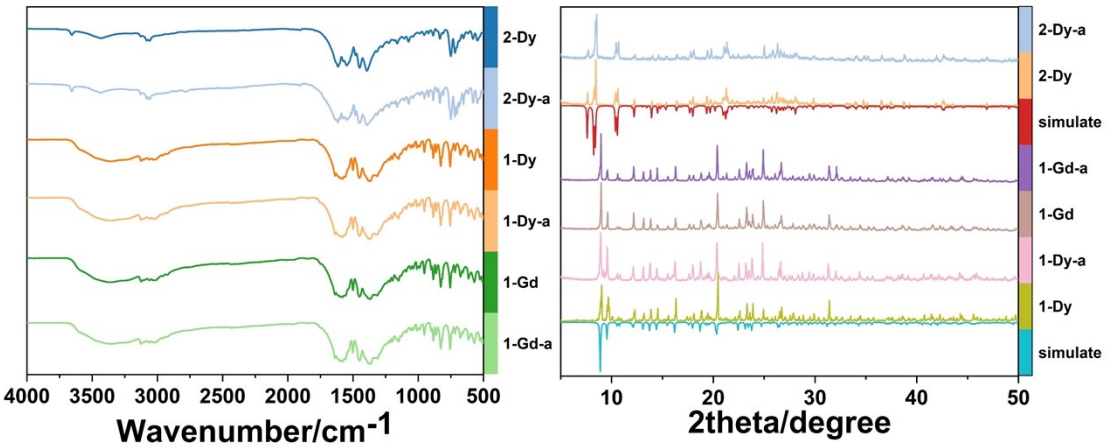

Fig. S3 IR and PXRD spectra of **1** and **2** before and after irradiation.

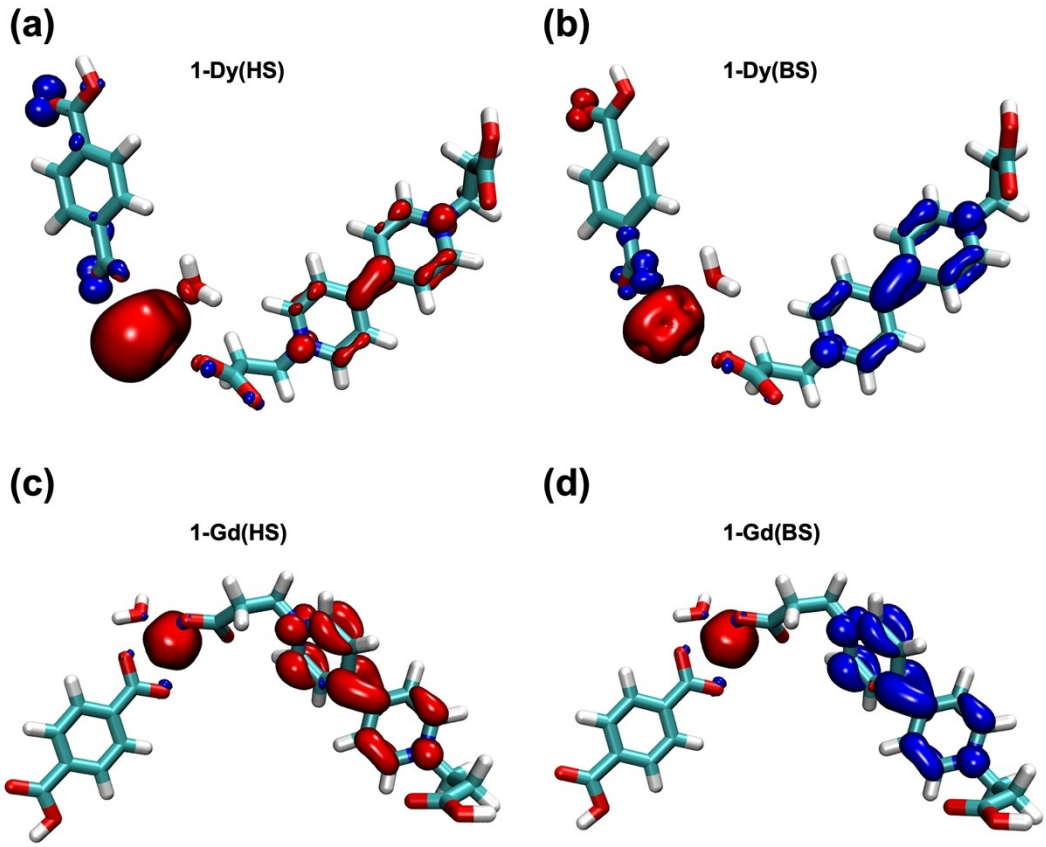

Fig. S4 The spin density isosurface plots of **1-Dy** and **1-Gd** in the High-Spin (a, c) and Broken Symmetry (b, d) states (red: alpha spin; blue: beta spin).

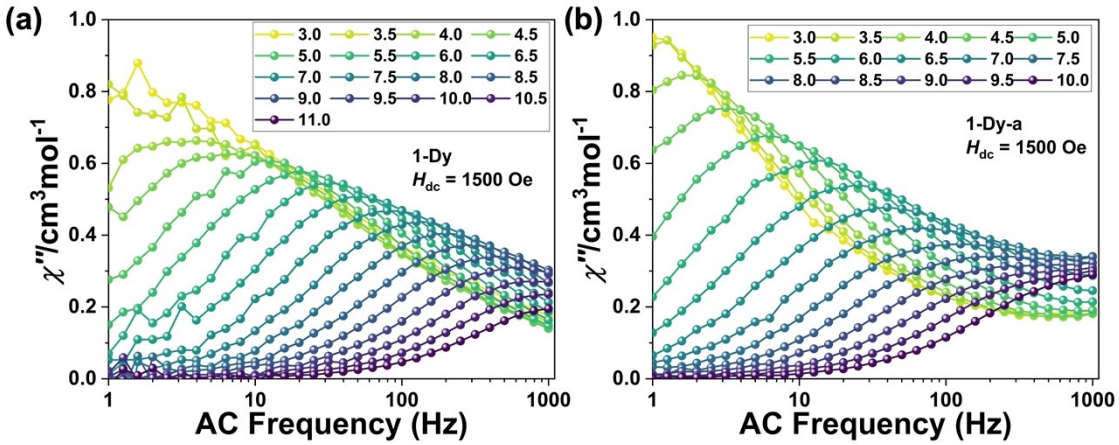

Fig. S5 Frequency dependence of the out-of-phase (χ'') components of **1-Dy** (a) and **1-Dy-a** (b) in 1500 Oe field between 3–11.0/10.0 K.

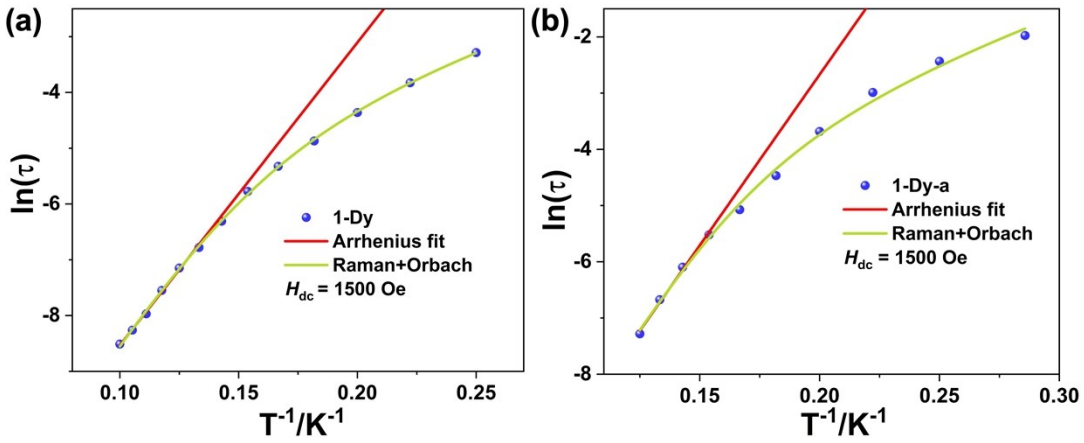

Fig. S6 Fitted curves for **1-Dy** (a), and **1-Dy-a** (b) based on the peak values of χ'' from the temperature-dependent ac susceptibility data.

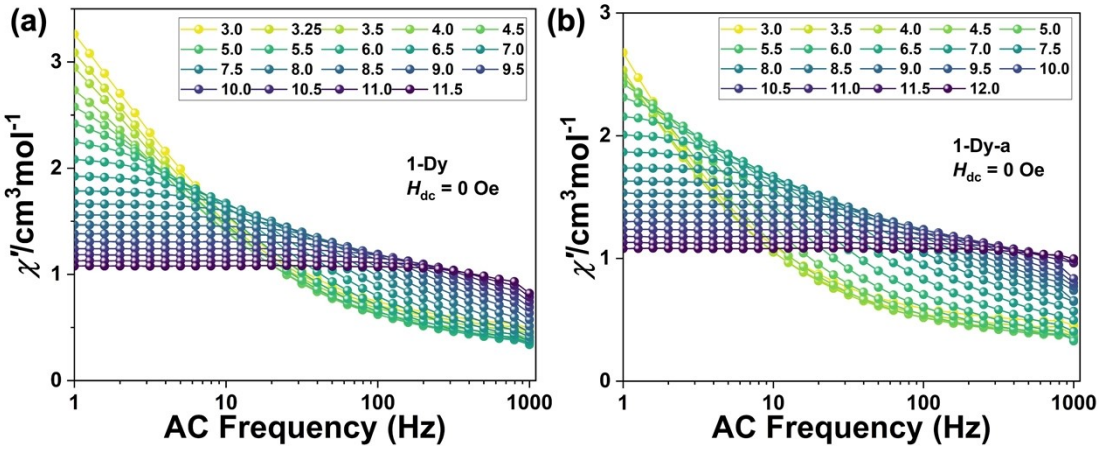

Fig. S7 Frequency dependence of the in-phase (χ') components of **1-Dy** (a) and **1-Dy-a** (b) in a zero-field between 3–11.5/12.0 K.

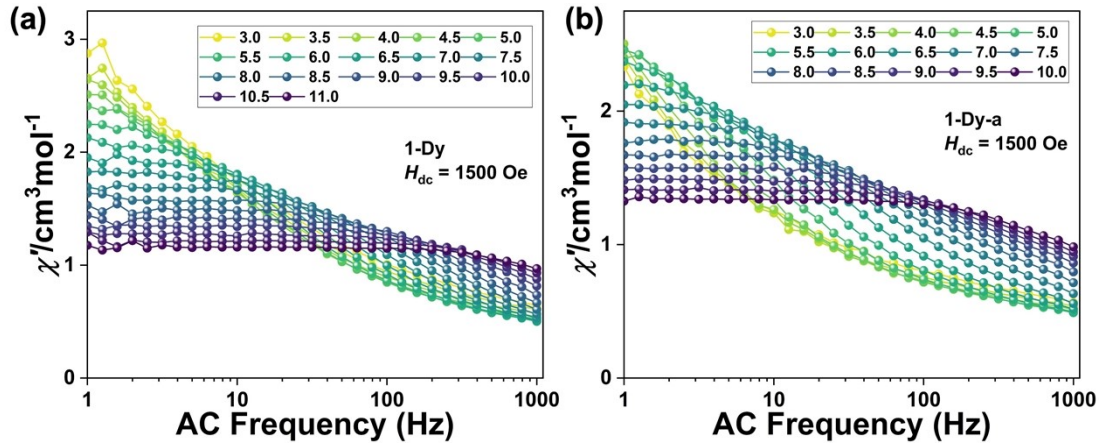

Fig. S8 Frequency dependence of the in-phase (χ') components of **1-Dy** (a) and **1-Dy-a** (b) in 1500 Oe field between 3–11.0/10.0 K.

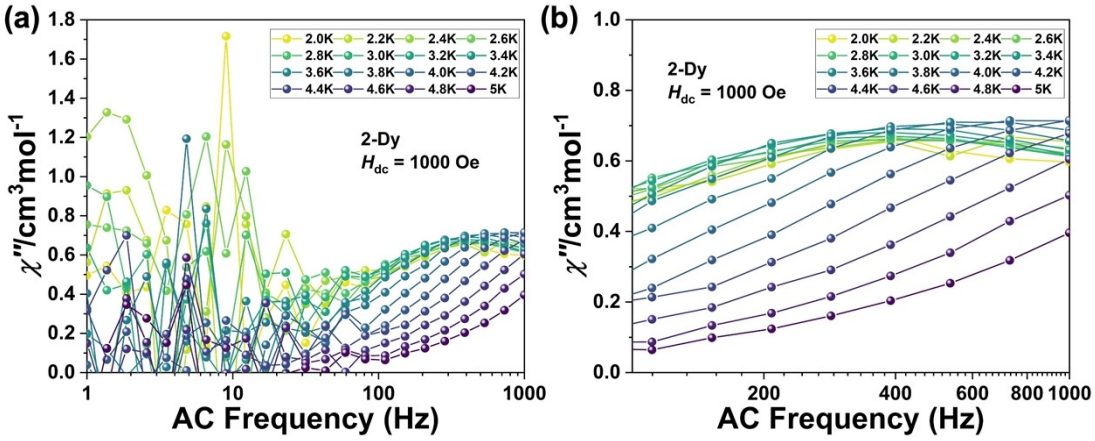

Fig. S9 (a) Frequency dependence of the out-of-phase (χ'') components of **2-Dy** in 1000 Oe field between 2.0-5.0 K, (b) an enlarged view of the 100-1000 Hz range.

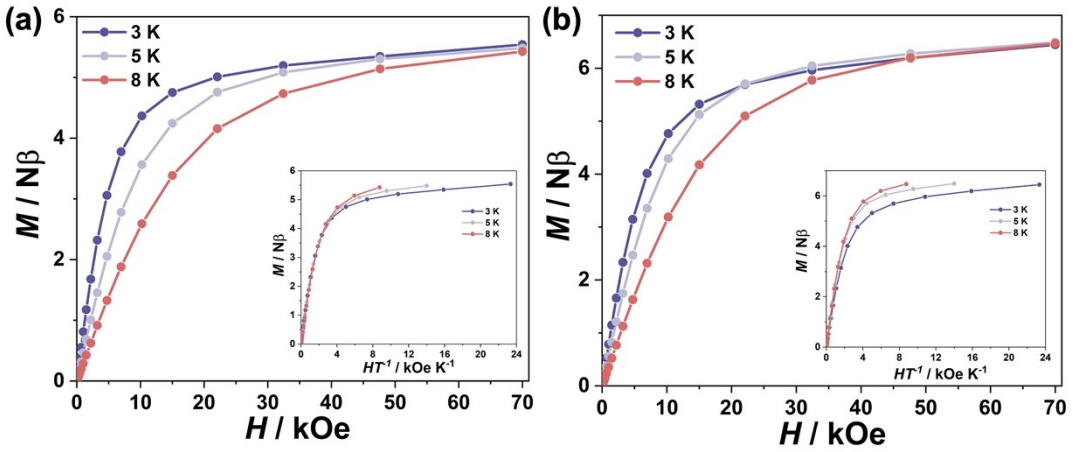

Fig. S10 Field dependence of the magnetization between 3 and 8 K for origin sample **1-Dy** (a) and colored sample **1-Dy-a** (b). (Inset: *M-H/T* curves of the samples before and after irradiation).

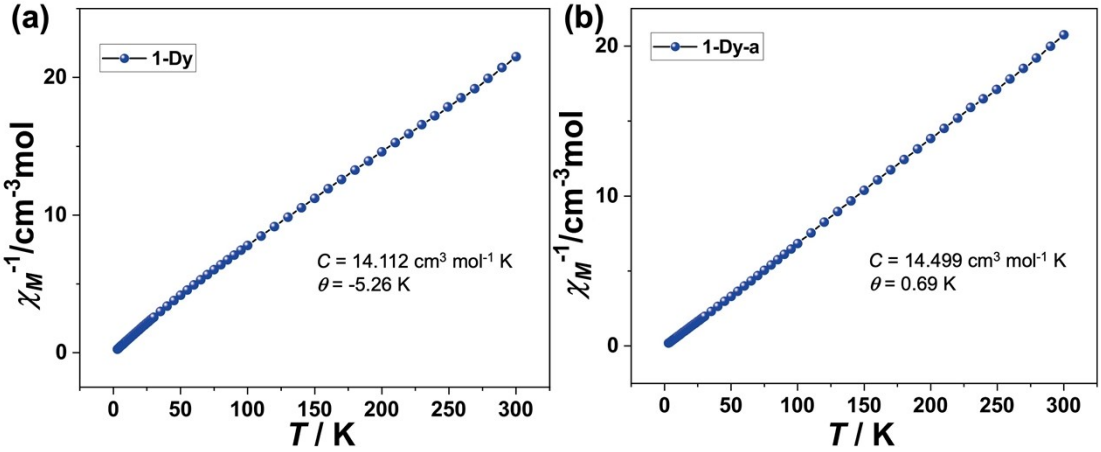

Fig. S11 χ_M^{-1} *versus T* plots for **1-Dy** (a), **1-Dy-a** (b).

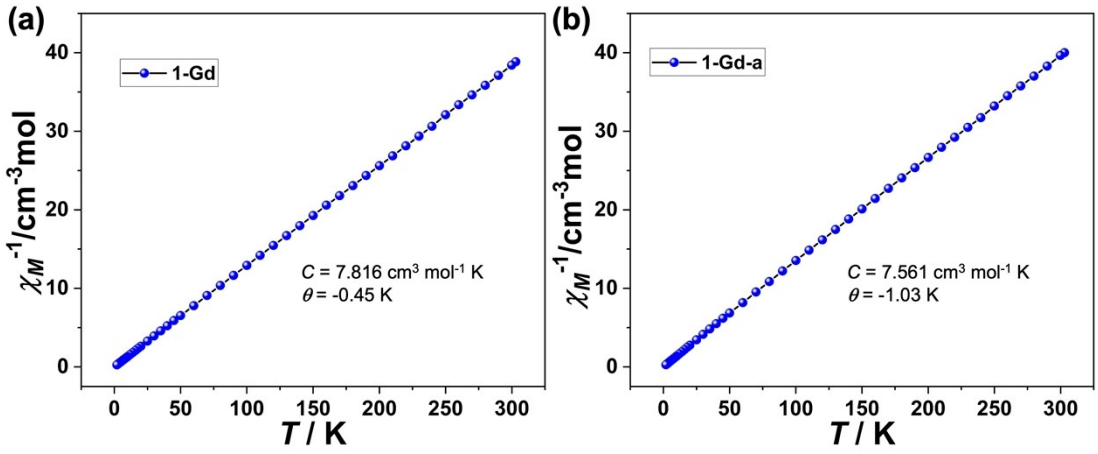

Fig. S12 χ_M^{-1} *versus* T plots for **1-Gd** (a), **1-Gd-a** (b).

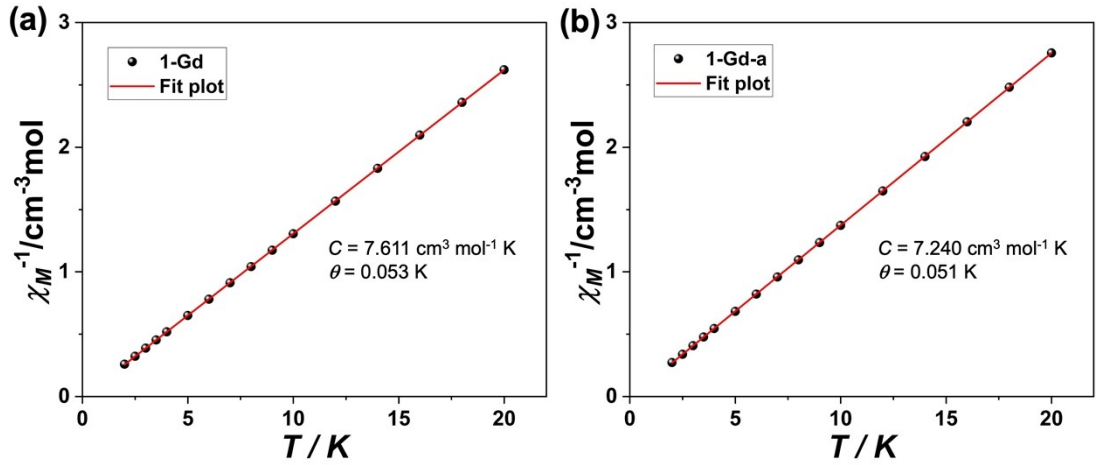

Fig. S13 χ_M^{-1} *versus* T plots for **1-Gd** (a) and **1-Gd-a** (b) were fitted using the Curie-Weiss law in the temperature range of 2–20 K.

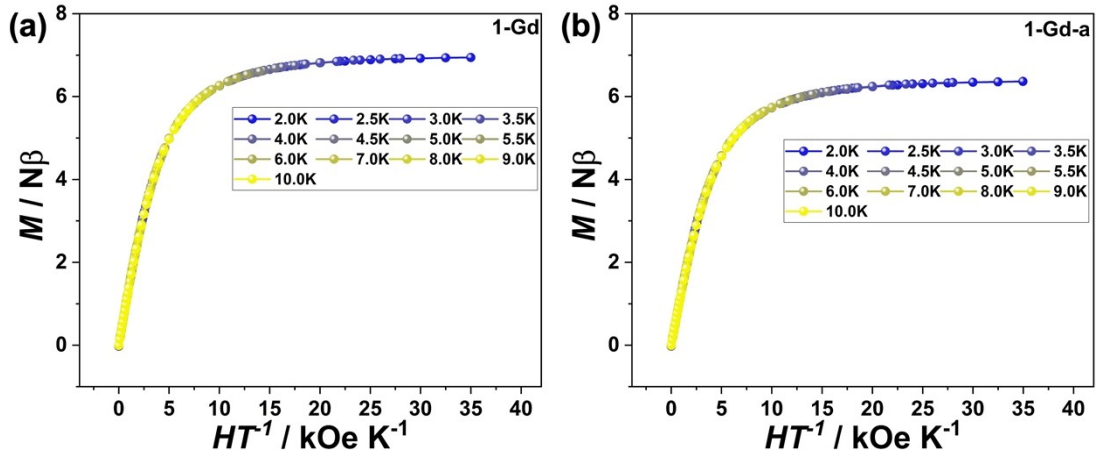

Fig. S14 *M versus* HT^{-1} plots for **1-Gd** (a) and **1-Gd-a** (b) at various temperatures (2-10 K).

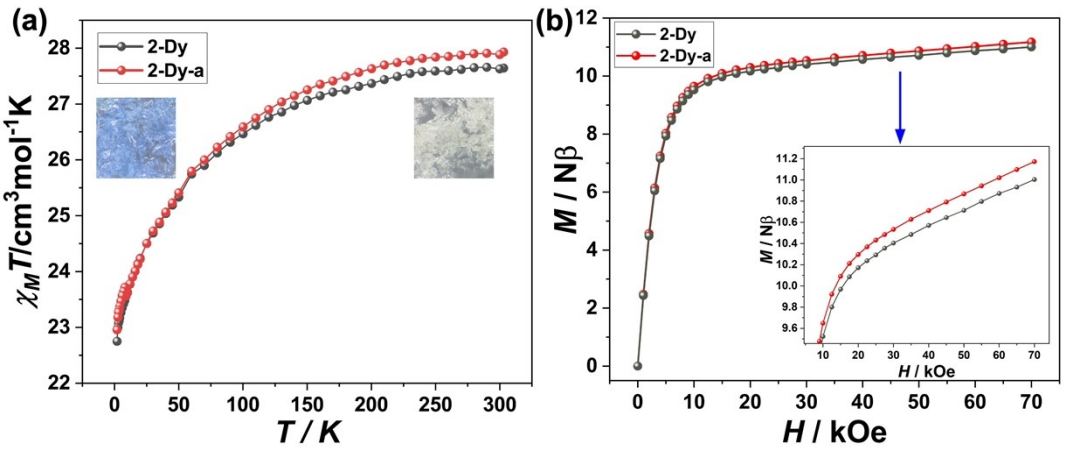

Fig. S15 (a) $\chi_M T$ *versus* T plots for **2-Dy**, **2-Dy-a**; (b) M-H curves of **2-Dy** and **2-Dy-a**.

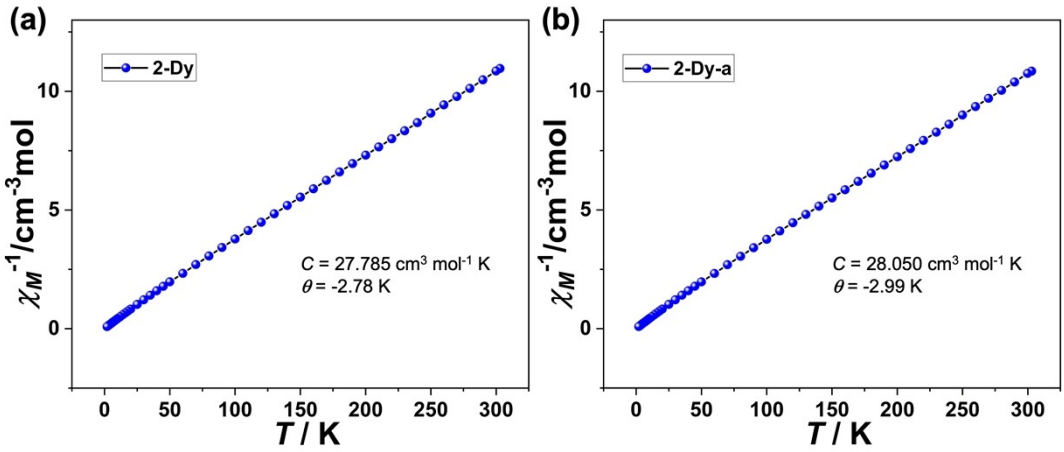

Fig. S16 χ_M^{-1} *versus* T plots for **2-Dy** (a), **2-Dy-a** (b).

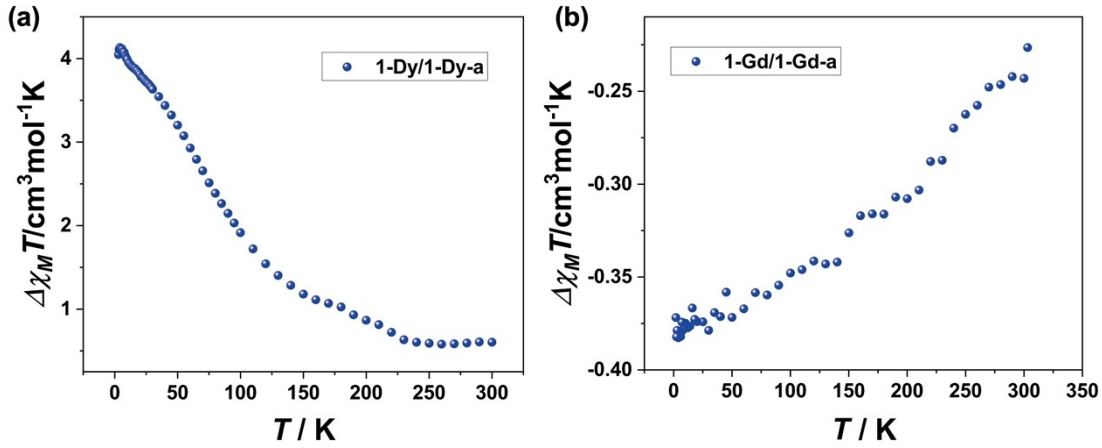

Fig. S17 The variation of $\chi_M T$ values between **1-Dy**, **1-Dy-a** and **1-Gd**, **1-Gd-a**($\Delta\chi_M T$).[11]

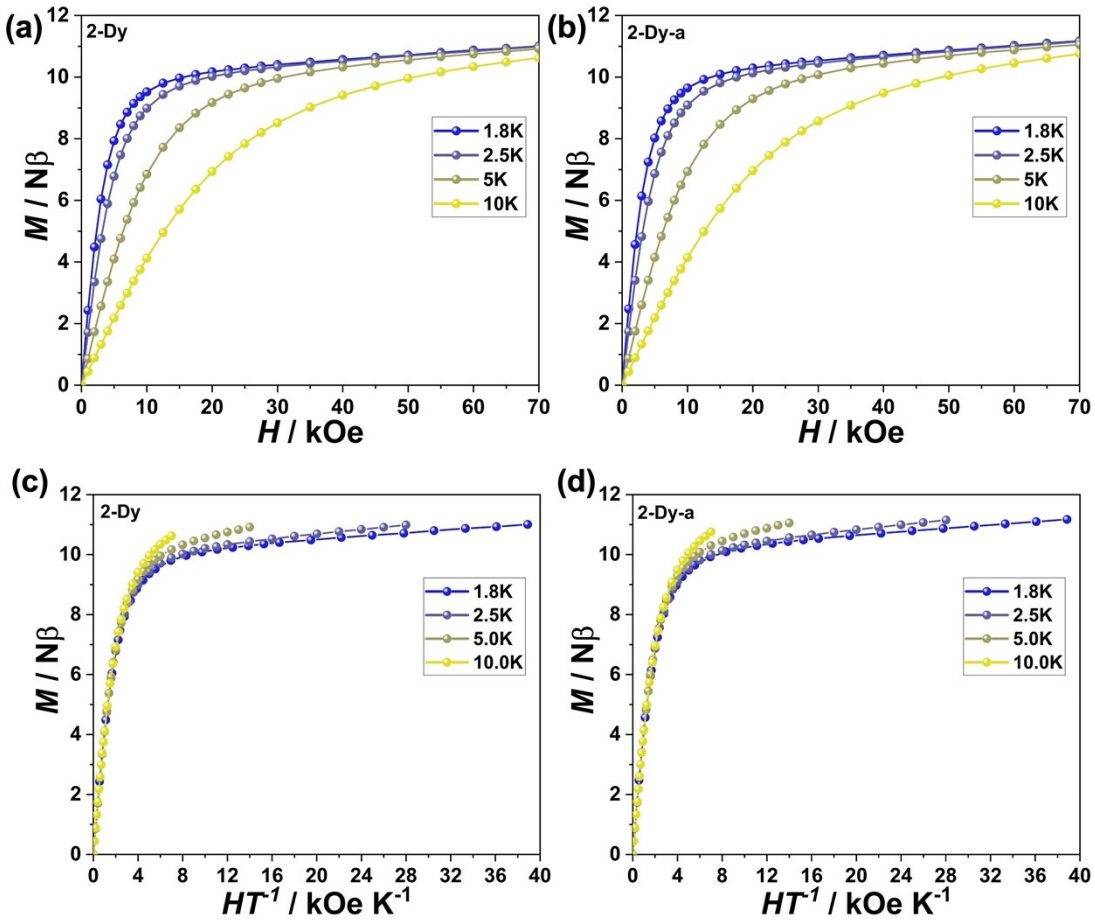

Fig. S18 *M versus H* plots for **2-Dy** (a) and **2-Dy-a** (b) at various temperatures (1.8-10 K); *M-H/T* curves of **2-Dy** (c) and **2-Dy-a** (d).

References

1. C. Sun, G. Xu, X.-M. Jiang, G.-E. Wang, P.-Y. Guo, M.-S. Wang and G.-C. Guo, *J. Am. Chem. Soc.*, 2018, **140**, 2805-2811.
2. H. Wang, X.-H. Sun, T.-T. Wang, Y.-X. Li, Y.-M. Xu and W.-B. Sun, *Chem. Commun.*, 2024, **60**, 12413-12416.
3. D.-D. Yang, Y.-S. Shi, T. Xiao, Y.-H. Fang and X.-J. Zheng, *Inorg. Chem.*, 2023, **62**, 6084-6091.
4. F. Neese, *WIREs. Comput. Mol. Sci.*, 2022, **12**, e1606.
5. F. Neese, F. Wennmohs, U. Becker and C. Riplinger, *J. Chem. Phys.*, 2020, **152**.
6. M. J. Frisch, G. W. Trucks, H. B. Schlegel, G. E. Scuseria, M. A. Robb, J. R. Cheeseman, G. Scalmani, V. Barone, G. A. Petersson, H. Nakatsuji, X. Li, M. Caricato, A. V. Marenich, J. Bloino, B. G. Janesko, R. Gomperts, B. Mennucci, H. P. Hratchian, J. V. Ortiz, A. F. Izmaylov, J. L. Sonnenberg, D. Williams-Young, F. Ding, F. Lipparini, F. Egidi, J. Goings, B. Peng, A. Petrone, T. Henderson, D. Ranasinghe, V. G. Zakrzewski, J. Gao, N. Rega, G. Zheng, W. Liang, M. Hada, M. Ehara, K. Toyota, R. Fukuda, J. Hasegawa, M. Ishida, T. Nakajima, Y. Honda, O. Kitao, H. Nakai, T. Vreven, K. Throssell, J. A. Montgomery Jr., J. E. Peralta, F. Ogliaro, M. J. Bearpark, J. J. Heyd, E. N. Brothers, K. N. Kudin, V. N. Staroverov, T. A. Keith, R. Kobayashi, J. Normand, K. Raghavachari, A. P. Rendell, J. C. Burant, S. S. Iyengar, J. Tomasi, M. Cossi, J. M. Millam, M. Klene, C. Adamo, R. Cammi, J. W. Ochterski, R. L. Martin, K. Morokuma, O. Farkas, J. B. Foresman and D. J. Fox, *Journal*, 2016.
7. T. Lu and F.-W. Chen, *J. Comput. Chem.*, 2012, **33**, 580-592.
8. T. Lu, *J. Chem. Phys.*, 2024, **161**, 082503.
9. K. Momma and F. Izumi, *J. Appl. Crystallogr.*, 2011, **44**, 1272-1276.
10. W. Humphrey, A. Dalke and K. Schulten, *J. Mol. Graph.*, 1996, **14**, 33-38.
11. P.-Y. Liao, Y. Liu, Z.-Y. Ruan, H.-L. Wang, C.-G. Shi, W. Deng, S.-G. Wu, J.-H. Jia and M.-L. Tong, *Inorg. Chem.*, 2023, **62**, 1075-1085.